scientific reports

Check for updates

OPEN

Experimental study of a fixed OWC-type wave energy converter in irregular wave conditions

Nicholas Ulm[1], Zhenhua Huang[1,3]✉ & Patrick Cross[2]

The experimental study of oscillating water column (OWC)-type wave energy converters (WECs) usually focuses on the performance of a WEC in regular wave conditions, as a function of available testing resources. This study examines the power performance of a fixed-geometry OWC that consists of a cylindrical OWC chamber affixed above a plate with V-shaped channels in irregular wave conditions. In evaluating power performance, different representative power take-off (PTO) damping values are considered. Using the data collected from a set of large-scale wave-basin tests, characterizing the quadratic damper relationship in regular and irregular wave conditions is examined, and the method using pressure as the sole measurement to calculate power extraction in irregular waves is assessed. Based on the observation of previous studies of OWCs in regular waves that the power extraction efficiency is not very sensitive to changes in wave amplitude if the wave period is fixed, a method is proposed to estimate the power performance of an OWC-type WEC in irregular wave conditions using results in frequency domain obtained in regular wave conditions. The method was verified using the data presented in this study and the data in the literature for the same WEC in regular wave conditions. The proposed method allows as OWC-type WEC designer to estimate the power extraction of an OWC-type WEC in irregular wave conditions using either experimental or numerical results in frequency domain obtained in regular wave conditions.

Keywords Wave energy, Oscillating water column, Power-at sea

Since the release of the U.S. Department of Energy's *Powering the Blue Economy* report[1], the US Navy and wave energy industry have begun a sincere investigation into how wave energy can benefit the marine industry through at-sea power production. The power range of a blue economy application ranges from 100 W to 10 kW, depending on the end use. Traditional approaches to powering activities at-sea treat the ocean as an "energy desert", where the energy resources are finite for the duration of a deployment. This had led to alternative thinking when it comes to the power requirements of wave energy converter (WEC) design. Previous efforts into wave energy have emphasized designs that can extract vast amounts of power from the most energetic conditions. As consistent power production for use in-situ becomes a new design application, the way that design optimization for wave energy needs to adjust. In order to redesign WEC types, iterative testing and prototyping may be needed, and thus more time and cost efficient methods of rapid development may be beneficial to improving WEC types.

The typical classification of WEC is determined by the energy extraction method, with each ranging in the degree of maturity of the technology[2]. These devices are typically classified by their extraction methods, such as attenuators, terminators, overtopping devices, point absorbers, surge converters, and more[3]. Among the various types of WECs, WECs based on oscillating water column (OWC) method are most studied. Broadly, OWC-type WECs can be classified as fixed OWCs and floating OWCs. Due to the simplicity of OWC designs, OWCs can be easily integrated with other structures for cost reduction[4,5]. A typical OWC-type WEC consists of a semi-submerged body with an enclosed pneumatic chamber commonly referred to as the OWC chamber. Inside the OWC chamber, there exists an internal air-water surface moving up and down as the incoming waves interact with and enters the chamber. The entrained mass of air is then forced through an opening, where a pneumatic power take-off (PTO) converts the focused kinetic energy of the air into rotational mechanical energy via a turbine[6]. The mechanical energy is then converted into electrical energy via a generator. Part of what makes OWC type WECs a more mature technology is the existence of a well-established industry surrounding the core aspects of the PTO, as the design and manufacturing of pneumatic turbines has long been a keystone industry in

[1]Department of Ocean and Resource Engineering, University of Hawaii at Manoa, Honolulu 96822, USA. [2]Hawaii Natural Energy Institute, University of Hawaii at Manoa, Honolulu 96822, USA. [3]These authors contributed equally: Nicholas Ulm and Zhenhua Huang. ✉email: zhenhua@hawaii.edu

the history of power production[7]. This concept was demonstrated previously in a number of applications, such as OWCs integrated with breakwaters[8] and coastal armaments[9], wave-powered navigation buoys[10]. For this reason and others, the Navy Expeditionary Warfare Center Marine Energy Development program has supported efforts to investigate the physics and power performance of an OWC-type WEC for ocean observing applications in remote and lower energy environments.

OWC-type WECs have been studied in field, experimentally, numerically and analytically. The scale of the model in experimental studies are often limited by the wave facility available, and Froude similarity is often used to design the experiment. Even through experimental studies can consider effects of viscosity and wave nonlinearity, Reynolds similarity and modeling laws related to air compressibility, however, are not satisfied. Therefore, model scales can induce additional uncertainty to the real power performance of an OWC system. In particular, the air compressibility may need to be considered for large scale models[11]. In general, the uncertainty introduced by scaling chamber height and PTO can be as much as 10%[12]. This uncertainty may change the rate of plateau to certain extent but would not change the conclusion qualitatively. Reliable data from the field or from large scale laboratory model tests are very useful for reducing uncertainty and accurately evaluating the performance of a OWC device at prototype scale. Due to the simplicity of OWC designs, OWCs can be easily integrated with other structures for cost reduction[4,5]. There are several prototype-scale examples of integrating OWCs with the coastal breakwater such as the one in Mutriku, Spain. The Mutriku coastal breakwater highlights the maturity of OWC technologies, as it has been in operation since 2011, and as of 2022 had delivered more than 2 GWh to the grid[13], and provides valuable filed data for OWC research. Time domain simulations of wave interaction with OWC-type WECs using Computational Fluid Dynamics (CFD) can be found in the literature[14–16]. Boundary Element Methods (BEMs) based on linear wave theory have also been widely used to analyze the wave interaction with OWC-type WECs in frequency domain[16]. Frequency-domain analytical studies of OWC-type WECs are also based on linear wave theory and suitable only for OWCs of simple geometry. Energy losses due to viscous effects such as vortex shedding from the structure are ignored in both analytical studies and BEM analysis, resulting in the predicted efficiency larger than the measured[16,17]. Currently, time-domain simulations of OWC-type WECs in irregular waves are still lacking due mainly to (1) the fact that it is still difficult to use the current computing technology to simulate 3D wave interactions with thin-walled structures for more than 500 waves and (2) the lack of quality experimental data for large-scale OWC models tested in a wave basin to calibrate the numerical models and verify the numerical results.

Ulm et al.[18]reviewed the role of geometric configurations in the previous literature and investigated the influence of different PTO damping on a novel geometry for ocean observing applications. It was highlighted that a geometry of particular interest is the spar shaped OWC, which is a hollow cylindrical semi-submerged structure that is partially or fully open at the bottom and can function as fixed or floating structure. The cylindrical structures are commonly used in both coastal and offshore applications, such as OWCs designed for use with breakwaters, piers, navigation buoys, and semi-submersible floating platforms. For this reason, their integration with existing infrastructure is of interest and has been previously investigated[8,19,20]. In the previous literature, most investigations have focused on shallow water conditions, which may not directly apply every application, as some are deployed in the intermediate water depth. The major challenge of deploying a standalone OWC in relatively deep water is the high cost associated with mooring or bottom fixing the structure. Co-location and integration of OWCs with new offshore infrastructure in intermediate water depth may be able to reduce the cost of installation. Since some ocean observing activities may be conducted in the intermediate water depth, such as observing around drilling platforms and fixed offshore wind farms[1,21], we will consider the fixed OWC designed as an ocean observing platform[18] to be deployed in the intermediate water depth in irregular wave conditions, with co-location and integration with new offshore infrastructure in mind.

Highlighted in Ulm et al.[18], it is often the objective of the previous literature to increase the efficiency of an OWC through describing the moonpool resonant frequency. Two metrics can describe the conversion mechanics of an OWC, namely the oscillatory volumetric flow rate and pressure response of an OWC system. The previous investigation by Ulm et al.[18] demonstrated that predictable OWC chamber dynamics could be achieved for a novel geometry and that a relationship can be made between pressure and volumetric flow rate to extraction efficiency through an analytical framework. Although capture efficiency can be important, an overemphasis on efficiency can overlook the primary objective of a WEC, which is to produce power. In Ulm et al.[18], capture efficiency was observed for a range of PTO damping values in regular wave conditions, and it was shown that the PTO damping with the greatest capture efficiency did not coincide with a meaningful increase in power production. Furthermore, it was demonstrated that the largest peak capture efficiency corresponded to a more narrow capture bandwidth, which may negatively impact power performance in site conditions with a wider band of available wave frequencies.

In the development of such a WEC technology, the relevant testing conditions are crucial in characterizing how that WEC will perform for a specific offshore power objective. The previous investigations into OWCs[22–24], and WECs more broadly, typically characterize power performance relative to a set of regular wave frequencies. Regular wave tests enable developers to understand the underlying physics of their device, as experimental results can be recreated in numerical wave tanks to demonstrate linear and nonlinear hydrodynamic effects[14,15]. These results can be useful in modelling power production and wave loading for a given wave frequency. Although practical in experimental and numerical testing, regular wave test can cause periodicity-induced phenomenon that may not occur in real seas, such as seiching due to vortex shedding[14].

Irregular wave tests can allow developers to assess performance of a WEC in more realistic conditions to an end application as they are defined by a spectrum of multiple wave frequencies. The majority of experimental studies employed orifice plates as a means of parameterizing the effects of a quadratic PTO, which has been well reviewed in the literature[7,14,22,25]. This is achieved with a coefficient of pressure loss, which is used to characterize the quadratic relationship of the velocity of the OWC chamber surface to the pressure drop observed across a

PTO[22]. It has been found that seiching inside the OWC chamber can influence the mean OWC chamber surface velocity measured using a wave probe, and thus affect the accuracy of the measured power production[14]. To reduce the influence of potential seiching in the measured efficiency, the previous investigations of WECs in regular wave conditions[14,18] suggested using the measured pressure alone to calculate the power extracted by an OWC.

Characterization of the orifice has been studied in steady flow conditions and regular wave conditions[22], but not in irregular wave conditions. The difference between steady flow condition and regular wave condition is that there is an asymmetric flow relationships between inhalation and exhalation of the OWC[26]. To enable the use of the pressure-alone method, we need assume instead an oscillatory flow relationship[18,22], which has not been demonstrated previously in irregular waves, to the authors knowledge. It is often the case that previous developers will measure airflow velocity via wave probes inside the OWC chamber or through direct measurement at the orifice, which can be onerous in model scale WEC development and requires specific types of bi-directional anemometers in the case of airflow measurement at the orifice. Instead, numerical methods have been used previously to validate the characterization of the orifice[27,28]. Numerical modeling of irregular wave conditions can be computationally expensive and thus limits the ability of WEC developers who do not have access to sufficient computational resources. The main difference between regular waves and irregular waves is that the seiching inside the OWC chamber may or may not exist in irregular wave conditions. In this study, we will assess the reliability of orifice characterization in regular waves relative to the found coefficient of fluidic loss found in irregular wave testing to determine the robustness of the methods previously used in Ulm et al.[18].

One method commonly employed is the use of transfer functions to define the frequency dependent response of each desired output[29]. In Oikonomou et al.[29], stochastic methods[30] of OWC turbine optimization were used to investigate a floating OWC in regular and irregular wave conditions. Oikonomou et al. presents the performance of the OWC from regular waves as a frequency dependent transfer function and makes a comparison of the overall performance of the WEC at discrete regular wave frequencies relative to the energy period of irregular wave conditions, which is about 0.9 times of the peak period for JONSWAP spectra[31]. The transfer functions generated were then used to validate the results of stochastic modeling of power performance in different sea states[29]. A similar application of this principle of generating a transfer function to model response in a wave spectrum has been demonstrated previously elsewhere[32,33]. What we propose in this study differentiates from the method of Oikonomou et al.[29], as we seek to verify a hypothesis that allows a developer to use the efficiency behavior of an OWC in regular wave conditions to estimate the OWC's efficiency behavior in different irregular wave conditions, and thus estimate the OWC's power extraction in different irregular waves conditions. The hypothesis is based on the observation of previous studies of OWCs in regular waves that the power extraction efficiency is not very sensitive to changes in wave amplitude if the wave period id fixed[4,18]. The motivation of the proposed method is the fact that obtaining a high resolution transfer function through irregular wave testing or time-domain simulations can be costly and time consuming in comparison and it is needed to have a simple approximate method to estimate the performance of an OWC in irregular waves so that it can be used to assist WEC designers with eliminating unpromising designs in the initial design stage. The objective of this study is to explore the possibility of using results from studies in frequency domain (experimental or analytical or BEM analysis) to provide such an approximation.

The selection of appropriate wave spectra for irregular testing can be used to generate appropriate transfer functions of WEC performance. For the purpose of applied WEC development, these conditions can and should be informed by site specific conditions, usually characterized as a wave spectrum, with a range of spectra possible[34].

The OWC-type WEC reported in this study is intended to be used at full scale at the Kilo Nalu Nearshore Observatory (KNO), which is on the south shore of Oahu, Hawaii. KNO functions as a power blue economy and small scale wave energy test bed that allows developers to deploy WECs in a relatively sheltered environment with on-site environmental monitoring cabled to shore. Site conditions at KNO are seasonally dependent, with long period swell present during most summer months and shorter period wind waves generated regionally year round. These conditions create a seasonally dependent bi-modal wave spectrum. Therefore, the irregular wave conditions used in this study are defined by a yearly-averaged spectrum measured at KNO.

Methods

In this section, we present the experimental setup of wave basin testing in irregular wave conditions, the methods used for orifice characterization in irregular waves, and the method proposed to estimate the performance of an OWC in irregular waves using results obtained in regular wave conditions.

Experimental setup

The OWC model, as show in Fig. 1, consists of a hollow cylindrical OWC chamber affixed above a submerged circular bottom plate and set of four rectangular wings affixed around the cylinder every 90 degrees. The model has the following characteristic lengths:

OWC chamber diameter D = 22 cm;
OWC chamber draft d = 44 cm;
Heave plate diameter D_h = 84 cm;
Thickness of OWC chamber t_{owc} = 3 mm;
Length of the wing l = 30.5 cm;
Diameter of the orifice D_o = 19 to 32 mm;
Thickness of the orifice plate δ = 8 mm;
Distance between the bottom plate and the OWC chamber h_{owc} = 16 cm;

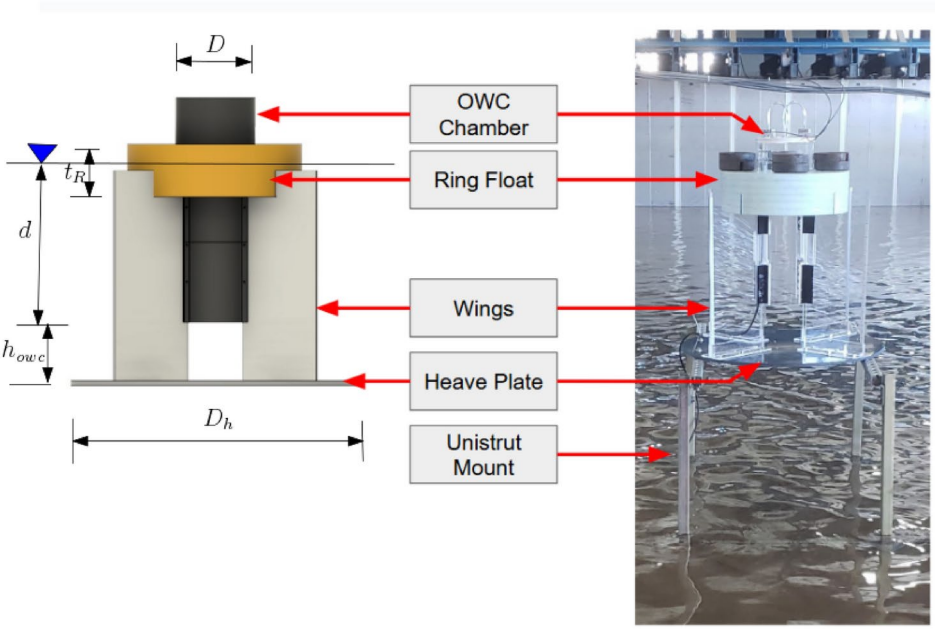


Fig. 1. Left: Side view of the model. Right: Image of the model in the half-drained basin.

Thickness of the top float t_R = 15 cm.

To represent the effects of a pneumatic power take off, orifice plates were manufactured and affixed to the top of the structure. Many authors[35,36] have previously described how the application of real pneumatic PTOs during scale testing is an impractical approach to developing OWC-type WECs. To maintain Froude similarity when scaling a pneumatic PTO, the previous literature has demonstrated that the use of parametric damping methods, such as sharp-edged orifice plates, is appropriate in recreating the effects of quadratic dampers[7,14,22,25]. In this test, a set of orifice plates were used with different opening ratios, $\alpha = D_o^2/D^2$. The set of acrylic orifice plates were professionally manufactured in accordance to ISO standard 5167-2[37]. Each orifice plate was sealed to the top surface of the OWC chamber using a silicone gasket adhesive, which was removed and reapplied each time an orifice plate was installed. Due to the limitation of time available at the wave basin, only 4 orifices were tested of $\alpha = [0.5\%, 0.7\%, 1.0\%, 1.5\%]$. The diameter orifices were based on the average optimal opening ratio found in the previous literature[18]. As turbine damping can be controlled via applied generator loading, the wide range of orifice diameters can provide insight into how future wave-to-wire control can be applied. The same model has been tested in regular wave conditions[18].

The OWC model was tested in the Directional Wave Basin at the O.H. Hinsdale Wave Research Laboratory (HWRL), Oregon State University. The basin layout is shown in Fig. 2. The basin is 48.8 m long and 26.5 m wide with a sloping beach at one end to absorb incident waves. The wavemaker for the Directional Wave Basin is a 30-channel piston-type belt-driven servomotor system with active wave absorption. A water depth of 1.36 meters was used for all tests.

The model was affixed 6.5 meters from the basin wall and tested concurrently with an identical floating model, 6.75 meters away. For the purpose of this study, we focus on the performance of the fixed model in irregular waves. A rosette of surface elevation probes were used to determine the incident surface elevation into the model, as well as a singular wave probe inside the OWC chamber. Two differential pressure sensors were used with a range of +/- 2488 Pascals, with an accuracy of 0.25% FS. Pressure sensors were chosen to be in-line with the direction of wave propagation. The manufacture-specified accuracy of the wave gauges is typically 0.1 mm. The sampling frequency used in the experiment was 100 Hz, which is much higher than the typical frequency of the water waves examined here.

Test wave conditions

The selection of appropriate wave spectra for irregular testing is important for resource characterization. There exist a number of wave measurement buoys around the island of Oahu that provide historical data sets that can be used to predict the conditions expected during ocean trials. The closest proximity data buoy available to KNO is NDBC 51211 (CDIP 233), which is a directional Waverider buoy originally deployed in 2017. In this study, a yearly-averaged spectrum measured by this buoy is used. The total history of spectra measured by this buoy were averaged for 2017 to 2019 to obtain the mean characteristic spectrum. The buoy is deployed in deeper water than the test site (35 meter water depth). In order to test the spectrum in the directional basin at Oregon State University, established Froude scaling principles[38] were applied to the field measurements, and the spectrum scaled to 1.36 m is shown in Fig. 3. KNO was originally established as a cabled observatory for coastal research at the University of Hawaii, investigating physical and biogeochemical processes of coral reefs[39]. As a part of the

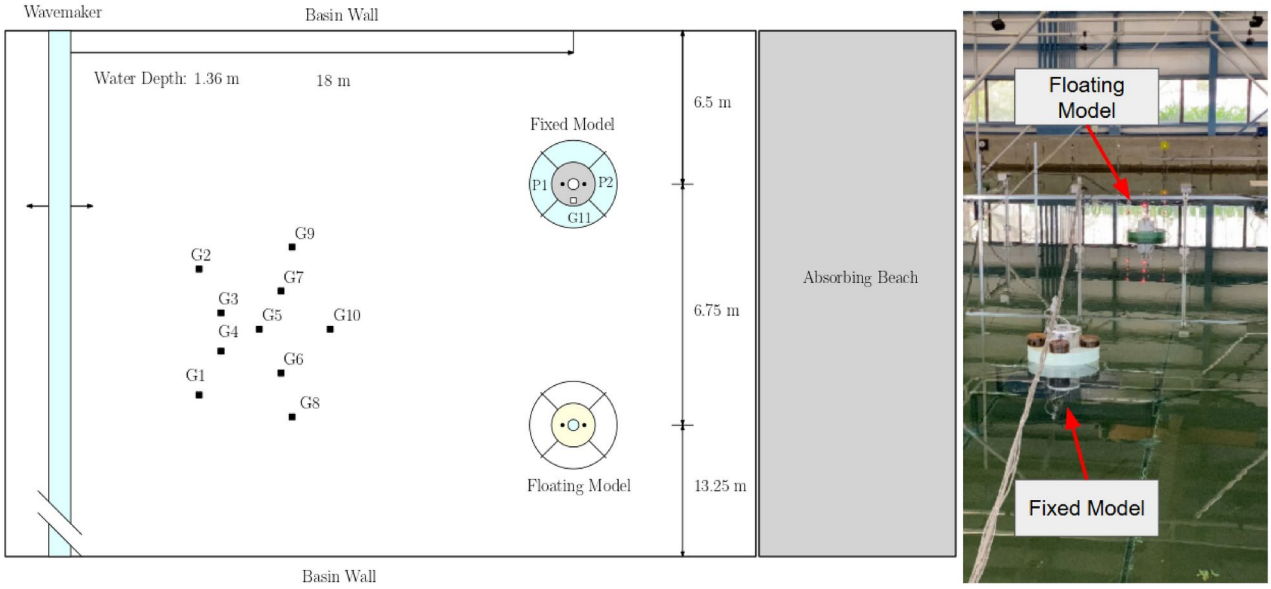


Fig. 2. Left: Top view of basin set Up (not to scale). G1–G11 represent surface elevation gauges, P1 and P2 represent pressure sensors. Right: Side image of the fixed and floating models in filled basin.

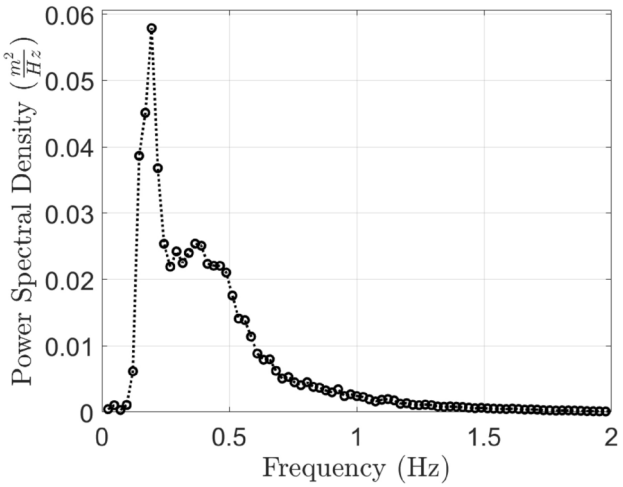


Fig. 3. Spectral density measured inside the basin and processed via Welch's periodogram method.

work at KNO[39], efforts were extended such that wave characteristics were measured with an acoustic doppler current profiler (ADCP) at the 10 meter water depth to inform the physical coastal processes. The ADCP data was collected from 2007 to 2010 and has been compared to the shoaled data from NDBC 51211 to verify that there is sufficient agreement. To generate a sufficient time series, a minimum of 800 waves were tested in the experiment.

Orifice characterization

The relationship between the pressure drop across an orifice plate in an oscillatory flow has been previously discussed in the previous literature[14,18,22]. OWC pressure inside the OWC air chamber can be expressed as a quadratic relationship with the spatially-average OWC chamber surface velocity $\overline{u}(t)$,

$$p(t) = \frac{C_f}{2}\rho_a|\overline{u}(t)|\overline{u}(t), \tag{1}$$

where $p(t)$ is instantaneous pressure drop across the orifice (i.e., the pressure relative to the atmospheric pressure) and C_f is the quadratic loss coefficient to be determined in the experiment. Semi-empirical expressions for C_f have been proposed for uniform and unidirectional pipe flow conditions[40] or regular sinusoidal oscillatory flow

conditions[14,18,22,41]. For steady flows or long waves, the following semi-theoretical expression for flow through sharp-edged orifices has been proposed[41]:

$$C_f = (\frac{1}{\alpha C_c} - 1)^2, \tag{2}$$

where C_c is an empirical flow contraction coefficient. However, the validity of Eq. (2) for irregular waves needs to be verified. In principle, C_f is a function of a Reynolds number *Re* and a frequency parameter in addition to the opening ratio[22]. For irregular waves, C_f can be determined using the measured $p(t)$ and $\overline{u}(t)$ through a least-square minimization by applying a Matlab non-linear curve fitting function *nlinfit* to Eq. (1). A sliding window method with 50% overlap was used to calculate the value of C_f for each orifice plate.

Error analysis

The C_f value determined by least-square fitting is then used to calculate the pressure using Eq. (1) to assess the goodness of fit. As we compare the goodness of fit of pressure or power production in the time series, we seek to assess the error and in some cases uncertainty of each using the R^2 and skill value of the time series. We define the model predictive skill[42] as follows,

$$Skill = 1 - \frac{\sum |Y_{fit} - Y_{obs}|^2}{\sum (|Y_{fit} - \overline{Y}_{obs}|^2 + |Y_{obs} - \overline{Y}_{obs}|^2)} \tag{3}$$

where Y_{fit} is the predicted variable time series and Y_{obs} is the observed value or measured time series. The overbar broadly represents the ensemble average of Y_{obs}.

Calculation of power extraction in irregular waves using pressure alone in time domain

For irregular waves, the average pneumatic power extraction per second can be found in the time domain performing a time averaging of instantaneous work done by the pressure force on the moving surface inside the OWC chamber, i.e.,

$$\overline{P_{OWC}} \approx \frac{1}{T_d} \int_{-T_d/2}^{T_d/2} P_{OWC}(t)dt, \quad P_{OWC}(t) = A_{OWC} p(t) u(t) \tag{4}$$

where $t = 0$ has been shifted to the middle of the time series, T_d is the duration of the time series, A_{OWC} is the cross-sectional area of the OWC chamber, and $P_{OWC}(t)$ is the instantaneous pneumatic power extracted by the OWC. This can be directly used to calculate the efficiency of the OWC using the incident wave power, $\overline{P_I}$, is known. The average efficiency of the OWC obtained using *p* and *u* is defined by

$$\epsilon_{pu} \equiv \frac{\overline{P_{OWC}}}{\overline{P_I} D}. \tag{5}$$

where the incident wave power can be calculated using incident wave spectrum $S_I(f)$,

$$\bar{P}_I = \rho g \frac{H_{rms}^2}{8} C_g(f_e) = \rho g \frac{A_{rms}^2}{2} C_g(f_e) = \rho g \int_0^\infty S_I(f) C_g(f) df, \tag{6}$$

where H_{rms} is the room-mean-square wave height, f_e the energy frequency[43], $S_I(f)$ the wave spectral density or wave energy spectrum of the incident waves, and $C_g(f)$ the group velocity for the component waves of frequency *f*. In signal analysis, it is called "signal power spectral density (sPSD)" or "power spectral density" (PSD) in short. For a measured time series of surface elevation change, the the wave spectral density or wave energy spectrum of the incident waves can be calculated using either Welch[44] or other periodogram[45,46] method. It is remarked that Oikonomou et al.[29] used a definition of efficiency same as the one defined in Eq. (5).

Assuming that the quadratic loss coefficient C_f is known, the pneumatic power extracted can be obtained using air pressure alone[18,22]. Since the air pressure inside the OWC chamber is related to the spatially-averaged velocity of the air flow by Eq. (1), the instantaneous pneumatic wave power $P_{OWC}(t)$ then can be expressed as

$$P_{OWC}(t) = A_{OWC} \sqrt{\frac{2}{\rho_a C_f}} |p(t)|^{3/2}. \tag{7}$$

Note that the total pneumatic power extracted is

$$P_{OWC}^{tot} \approx \int_{-T_d/2}^{T_d/2} P_{OWC}(t)dt, \tag{8}$$

and such that the extraction efficiency obtained using pressure alone can be approximated by

$$\epsilon_p \approx \int_{T_d/2}^{T_d/2} \frac{P_{OWC}(t)}{\bar{P}_I D} dt. \tag{9}$$

which can be used for regular and irregular waves. For regular waves, we can take T_d as one or several wave periods. This time domain representation of efficiency, although useful, does not give a clear picture of the frequency dependence of extraction efficiency, which is useful to a WEC designer to optimize a WEC design. In the following we present a method to estimate the power extraction efficiency in irregular waves using results from regular waves in the frequency domain.

Estimation of power extraction in irregular waves using results from regular waves in frequency domain

To develop the method for calculating the power extraction in frequency domain, we will take $T_d \to \infty$ for now. The instantaneous wave power extraction $P_{OWC}(t)$ normalized by $P_{OWC}^{tot} D$ can be written using $|p(t)|$ as follows

$$\frac{P_{OWC}(t)}{P_{OWC}^{tot}} = X_{1/2}(t)^2 = |X_{1/2}(t)|^2, X_{1/2}(t) = \sqrt{\xi |p(t)|^{3/2}}, \quad \xi = \frac{A_{OWC}}{P_{OWC}^{tot}} \sqrt{\frac{2}{\rho_a C_f}}. \tag{10}$$

It then follows that

$$\int_{-\infty}^{\infty} |X_{1/2}(t)|^2 dt = 1, \tag{11}$$

Let denote the the spectrum of $X_{1/2}(t)$ as

$$\hat{X}_{1/2}(f) \equiv \int_{-\infty}^{\infty} X_{1/2}(t) e^{-i2\pi f t} dt. \tag{12}$$

Since $X_{1/2}(t)$ is a square-integrable function on $[-T_d/2, T_d/2]$ with $T_d \to \infty$, according to Parseval's theorem[47], we have

$$\int_{-\infty}^{\infty} |X_{1/2}(t)|^2 dt = \int_{-\infty}^{\infty} |\hat{X}_{1/2}(f)|^2 df = \int_0^{\infty} 2|\hat{X}_{1/2}(f)|^2 df = 1 \tag{13}$$

where the factor 2 is introduced because$|\hat{X}_{1/2}(f)| = |\hat{X}_{1/2}(-f)|$ and Eq. (11) has been used.

In view of Eq. (13), we have the following self-explanatory identity:

$$P_{OWC}^{tot} = 2 \int_0^{\infty} P_{OWC}^{tot} |\hat{X}_{1/2}(f)|^2 df. \tag{14}$$

Physically, the factor $2|\hat{X}_{1/2}(f)|^2$ determines how the wave power is extracted by each frequency component across the frequency spectrum. It then follows that the pneumatic power extracted by the frequency component f within a frequency bin of Δf is

$$P_{OWC}^{Irr}(f) \equiv 2 P_{OWC}^{tot} |\hat{X}_{1/2}(f)|^2 \Delta f \tag{15}$$

If we perform tests using regular waves of frequency f, we can approximate the spatially-averaged velocity of the air flow inside the OWC chamber $u(t)$ by

$$u(t) = \hat{U} \cos(2\pi f t + \psi) \tag{16}$$

where $\hat{U}$ is the amplitude and ψ the corresponding phase angle of $u(t)$. Using the equation for the orifice, Eq. (1), we have

$$p(t) = \frac{1}{2} \rho_a C_f \hat{U}^2 |\cos(2\pi f t + \psi)| \cos(2\pi f t + \psi). \tag{17}$$

and

$$p(t)u(t) = \frac{1}{2} \rho_a C_f \hat{U}^3 |\cos(2\pi f t + \psi)|^3. \tag{18}$$

It then follows that the period-averaged pneumatic power extraction P_{OWC}^{Reg} is

$$P_{OWC}^{Reg} = A_{OWC} \overline{p(t)u(t)} = A_{OWC} \frac{2}{3\pi} \rho_a C_f \hat{U}^3, \tag{19}$$

where $\overline{|\cos(2\pi ft+\psi)|^3} = 4/3\pi$ has been used.

To linearize the orifice equation, Eq. (1), we introduce a linear coefficient κ such that

$$p(t) = \kappa\frac{1}{2}C_f\rho_a\hat{U}u(t) = \kappa\frac{1}{2}C_f\rho_a\hat{U}^2\cos(2\pi ft+\psi) \equiv \hat{P}\cos(2\pi ft+\psi), \tag{20}$$

where $\hat{P}$ is defined as

$$\hat{P} \equiv \kappa\frac{1}{2}C_f\rho_a\hat{U}^2 \tag{21}$$

To determine the value of κ, we recall that the period-averaged pneumatic power extraction based on the linearized pressure is

$$A_{OWC}\overline{p(t)u(t)} = A_{OWC}\kappa\frac{1}{2}C_f\rho_a\hat{U}^3\overline{|\cos(2\pi ft+\psi)|^2} = A_{OWC}\frac{\kappa}{4}C_f\rho_a\hat{U}^3 \tag{22}$$

where $\overline{|\cos(2\pi ft+\psi)|^2} = 1/2$ has been used. Comparing Eqs. (19) and (22) gives

$$\kappa = \frac{8}{3\pi}. \tag{23}$$

It then follows from Eq. (21) that

$$\hat{P} = \frac{8}{3\pi}\frac{1}{2}C_f\rho_a\hat{U}^2, \text{ or } \hat{U} = \frac{1}{2}\sqrt{\frac{3\pi}{\rho_aC_f}}\hat{P}^{1/2}. \tag{24}$$

In view of Eq. (19), the period-averaged power extracted by the OWC in regular waves of frequency f can be re-written as

$$P_{OWC}^{Reg} = \frac{\sqrt{3\pi}}{4}A_{OWC}\sqrt{\frac{1}{\rho_aC_f}}\hat{P}^{3/2}. \tag{25}$$

Similar to the definition of ϵ_{pu} given in Eq. (5), we denote the power-extraction efficiency obtained using regular waves of frequency f as

$$\epsilon_{Reg}(f) \equiv \frac{P_{OWC}^{Reg}}{P_ID}, \tag{26}$$

where the incident wave power for regular waves of amplitude A_I can be calculated by $P_I = \rho gC_gA_I^2/2$. If $\epsilon_{Reg}(f)$ is known for an OWC, P_{OWC}^{Reg}, the power extracted in waves with an incident power P_I, can be calculated by

$$P_{OWC}^{Reg} = \epsilon_{Reg}(f)P_ID \tag{27}$$

When testing an OWC in regular waves, it has been found in the literature that $\epsilon_{Reg}(f)$ is not very sensitive to variation in wave amplitude in the range of interest if the wave frequency is fixed[4,18].

For irregular waves of a spectrum $S_I(f)$, the amplitude of the component wave associated with frequency f, A_I, can be calculated by $S_I(f)C_g(f)\Delta f = A_I^2/2$ with Δf being a frequency bin[48]. Therefore, the power of the component wave of frequency f within a frequency bin Δf is

$$P_I = \rho gC_g(f)A_I^2/2 = \rho gS_I(f)C_g(f)\Delta f \tag{28}$$

We denote the pneumatic power extracted by this component wave as $P_{OWC}^{Reg}(f)$. The fact that $\epsilon_{Reg}(f)$ is not very sensitive to wave amplitude as found in the literature[4,18] allows us to

1. Use the expression for P_I given in Eq. (28) to replace P_I in Eq. (27) so that

$$P_{OWC}^{Reg}(f) \equiv \epsilon_{Reg}(f)\left[D\rho gS_I(f)C_g(f)\Delta f\right] \tag{29}$$

within the range of wave frequencies tested in regular wave conditions.

2. Hypothesize that Eq. (15) can be approximated by Eq. (29), i.e.

$$P_{OWC}^{Irr}(f) \approx P_{OWC}^{Reg}(f), \tag{30}$$

which means

$$P_{OWC}^{tot}\left(2|\hat{X}_{1/2}(f)|^2\Delta f\right) \approx \epsilon_{Reg}\left[D\rho g S_I(f)C_g(f), \Delta f\right] \tag{31}$$

or

$$2P_{OWC}^{tot}|\hat{X}_{1/2}(f)|^2 \approx \epsilon_{Reg}(f)\left[D\rho g S_I(f)C_g(f)\right]. \tag{32}$$

within the range of wave frequencies tested in regular wave conditions.

Equation (32) can be rewritten as

$$\boxed{\epsilon_{Irr}(f) \equiv \frac{2P_{OWC}^{tot}|\hat{X}_{1/2}(f)|^2}{D\rho g S_I(f)C_g(f)} \approx \epsilon_{Reg}(f)}. \tag{33}$$

within the range of wave frequencies tested in regular wave conditions.

Physically, we hypothesize that $\epsilon_{Irr}(f)$, the frequency dependent extraction efficiency found by a component waves of frequency f in irregular waves, can be approximated by $\epsilon_{Reg}(f)$, the extraction efficiency found in regular waves of the same same frequency.

One of the objectives of this work is to test the hypothesis using the data from large-scale wave basin tests on the same model under regular and irregular waves. If this hypothesis can be tested true, we can obtain from Eq. (33) that the total power extracted P_{OWC}^{tot} in irregular waves can be approximate by $\tilde{P}_{OWC}^{tot}$:

$$\tilde{P}_{OWC}^{tot} \approx \int_0^\infty \epsilon_{Reg}(f)\left[D\rho g S_I(f)C_g(f)\right] df, \tag{34}$$

Therefore, the efficiency of the OWC in irregular waves can be approximated by $\tilde{P}_{OWC}^{tot}/(P_I D)$, i.e., we can approximate ϵ_{pu}, the efficiency of an OWC in irregular waves given in Eq. (5), by $\tilde{\epsilon}_p$ calculated by

$$\tilde{\epsilon}_p = \frac{\tilde{P}_{OWC}^{tot}}{P_I D} \tag{35}$$

Oikonomou et al.[29] also presented a approach for using regular wave condition results to model average power performance in different irregular wave conditions, but they didn't use the hypothesis introduced here for component waves. It was previously shown that some agreement occurs between the use of regular wave results to model irregular wave performance, the assessment was limited to findings of energy period f_e rather than frequency dependent performance. The hypothesis introduced here seeks to demonstrate that not only can regular wave results be used, but in fact the regular wave transfer function $\epsilon_{Reg}(f)$ may sufficiently replicate the frequency dependent transfer function $\epsilon_{Irr}(f)$ found via irregular wave conditions, which allows a WEC developer use regular wave results to perform preliminary optimization of an OWC for a targeted irregular wave condition as explained in the Discussion section later.

Results

In this section, we present the results of the wave basin testing of the OWC in irregular wave conditions. We assess characterization of the orifice under regular and irregular conditions, evaluate the agreement of using pressure to estimate the average extraction efficiency of the WEC, and test the hypothesis that the power extraction of an OWC in irregular waves can be approximated by using the efficiency obtained in regular waves.

Orifice characterization

Orifice characterization is presented to estimate the quadratic loss coefficient C_f, which is a representation of the relationship between the surface velocity of the water inside the OWC chamber and the differential pressure across the orifice. Knowledge of the value of C_f, which characterizes PTO damping, is important as it allows us to evaluate the efficiency of an OWC using pressure alone via Eq. (7). This is beneficial when the WEC developer may not be able to measure both pressure and surface velocity reliably, which is specially true for floating OWCs. However, the accuracy of the power extraction calculated using Eq. (7) relies on the accuracy and reliability of C_f to represent the quadratic relationship.

Previous studies[7,14,22,25] have primarily focused on this relationship via monochromatic oscillations in airflow and as such, does not assess how the introduction of irregular oscillatory flow may impact the estimation of C_f . Assessing possible influence of wave irregularity on the experimentally-determined values of C_f is important due to the following considerations: (i) The influence of sloshing or seiching can be of concern when using regular waves to characterize this quadratic relationship[14,18], but irregular conditions reduce the likelihood of periodicity-induced phenomenon; (ii) OWCs can have asymmetric flow relationships between inhalation and exhalation of the OWC[26]; (iii) it has been found that the values of C_f obtained in regular wave conditions are weakly depended on wave period[22]. Therefore, it is not clear to what the extent the wave irregularity may affect the values of C_f used to parameterize the pressure-velocity relationship.

Sample pressure and surface elevation measured inside the OWC chamber are presented in Fig. 4 for $\alpha = 1.0\%$, where the pressure parameterized using Eq. (1) is also included for comparison. It can be seen that the agreement between the parameterized and measured pressure is very well, with a R^2 value of 0.9508 and a

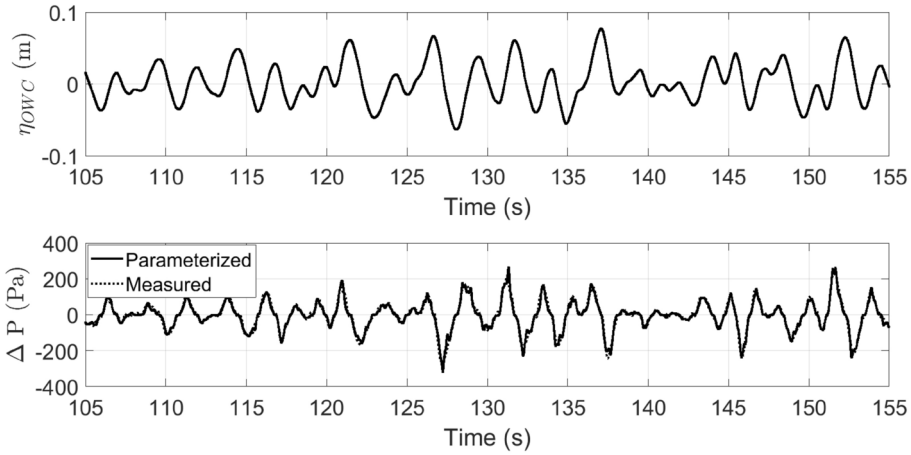


Fig. 4. Sample time series of (Top) instantaneous surface elevation inside the OWC chamber and (Bottom) Fitted and Measured Differential pressure for $\alpha = 1.0\%$.

Opening ratio α (%)	R^2	Skill	C_f^{Reg} (10^4)	C_f^{Irr} (10^4)
0.5	0.9178	0.9781	6.9543	7.5520
0.7	0.9292	0.9813	3.9217	3.9277
1.0	0.9508	0.9872	2.0259	2.0319
1.5	0.9565	0.9882	0.9640	0.9900

Table 1. R^2 and skill values quantifying the agreement between the measured pressure and the pressure parameterized using C_f^{Irr} in irregular conditions. The value of C_f obtained using regular waves are included as C_f^{reg} for comparison.

skill value of 0.9872. The values of C_f obtained in irregular wave is $2.0259\times^{-4}$ for this case, while the values of C_f obtained in regular wave conditions[18] is $2.0319\times^{-4}$. The values of C_f obtained in regular and irregular wave conditions for other opening ratios, together with the R^2 and skill values are presented in Table 1, where it is shown that there is broad agreement between the values of C_f. The fact that the values obtained in irregular cases being slightly larger those obtained in regular wave conditions is possibly due to wave-induced seiching inside the OWC chamber, which is a period-related phenomenon[17] and thus may not be present in irregular wave conditions. The broad agreement of C_f across orifices is reinforced by the fact that the parameterized pressure using the surface velocity broadly agrees with the measured pressure signal, such that the R^2 and Skill values are above 0.9 for all orifices. The largest disagreement in C_f occurs in the smallest orifice, which is expected, as the largest variation of period-averaged C_f were observed previously[18] for $\alpha = 0.5\%$. This may be because the smallest investigated orifice, $\alpha = 0.5\%$, is at the cusp of what is defined as 'sharp-edge orifice' and that seiching was observed in higher frequency regular wave cases. In the irregular wave condition, periodicity-induced seiching should not be present in general, and as such, an over approximation from seiching would result in a lower C_f.

Two methods for calculating extraction efficiency calculated in time domain

To confirm that pressure alone can be used to evaluate the extraction efficiency of an OWC in irregular wave conditions, we examine the time-averaged extraction efficiency for the entire test by comparing the extracted power obtained using Eq. (4) with the extracted power obtained using pressure solely via Eq. (7). It is seen in Table 2 that the method using pressure alone consistently finds the efficiency to be 4-5 % greater than that found using pressure and surface velocity. The largest disagreement occurs with the $\alpha = 0.5\%$, which aligns with the trend found previously for characterizing C_f. This would imply that the use of pressure alone may be sufficient to characterize extraction efficiency for orifices and that orifices on the cusp of the 'sharp-edge' definition may have about 5% uncertainty.

Calculation of extraction efficiency in frequency domain

It is often the first instinct of an engineer that the efficiency of a WEC in regular wave conditions may be used as a characteristic representation of efficiency for an equivalent irregular wave condition. This is to say that regular wave conditions can approximate the average efficiency of a WEC in a spectrum at a single regular wave frequency using a characteristic wave height for that frequency. A difficulty in this is defining an equivalent characteristic wave height and period of the spectrum for this purpose. Let us use the example of root-mean square wave height (H_{rms}) and mean-zero crossing period (T_z). H_{rms} represents the characteristic mean

Opening ratio α (%)	ϵ_p	ϵ_{pu}	$[\epsilon_p - \epsilon_{pu}] / \epsilon_{pu}$
0.5	0.0383	0.0363	0.0567
0.7	0.0389	0.0371	0.0481
1.0	0.0345	0.0331	0.0411
1.5	0.0285	0.0273	0.0426

Table 2. Time-averaged extraction efficiency via each method, and the percent difference found. ϵ_p represents the time-averaged efficiency using pressure only via Eq. (9) and ϵ_{pu} represents the time-averaged efficiency using pressure and measured surface elevation via Eq. (5).

wave height of the spectrum while T_z represents the mean wave period observed. For the presented spectrum examined in our wave-basin tests , the characteristic wave height $H_{rms} = 7.7$ cm and period $T_z \approx 2$ seconds can be used. If we look at $\alpha = 1.0\%$, the regular wave efficiency found in Ulm, et al.[18] is estimated to be $\epsilon = 0.15$. The average measured efficiency in the presented spectrum can be seen in Table 2, showing that this approach poorly estimates the performance of the spectrum. This highlights that the average efficiency of a WEC in irregular wave conditions cannot be defined by a single frequency.

A higher fidelity method of extraction efficiency estimation for a given WEC in irregular wave conditions might be to create a frequency dependence function for "extraction efficiency", $\epsilon(f)$, which is related to a transfer function of the instantaneous power extracted normalized by the power spectrum of incident waves. In cases where the WEC developer can accurately estimate the spatial average of surface velocity inside the OWC chamber, the measured differential pressure signal and surface elevation can be used in Eq. (5) to determine the averaged efficiency exactly. However, accurately measuring the spatially-averaged surface velocity inside the OWC chamber can be difficult due to a number of constraints, especially the non-uniformity of the water surface inside the OWC chamber[14] and the relative motion of the WEC to waves in the case of a floating OWC. We know from the previous section that the use of the pressure signal alone can provide a very good approximation to the average extraction efficiency in the time domain. In this section, we will use the data from our large scale tests in a wave basin under irregular wave conditions to test the hypothesis stated in Eq. (33). The confirmation of the hypothesis is important as WEC developers may not always have access to facilities capable of generating irregular wave conditions and performing numerical simulations using irregular waves is still a challenge at the current computing technology. Therefore, there is a need for an approach which allows developers to approximately evaluate the performance of an OWC in irregular wave conditions using results obtained using regular waves.

To test the hypothesis stated by Eq. (33), we compare the efficiency found from regular wave tests for each frequency $\epsilon_{Reg}(f)$ to $\epsilon_{Irr}(f)$ obtained from irregular wave tests for the same OWC model. The comparison is shown for each orifice in Fig. 5, where we can see that $\epsilon_{Reg}(f)$ has acceptable agreement with $\epsilon_{Irr}(f)$ for all cases tested, as indicated by visual observation and the R^2 and Skill values listed in Table 3.

In addition to the R^2 and Skill values, we should also compare the average extraction efficiency ϵ_p calculated by Eq. (9) and $\tilde{\epsilon}_p$ by Eq. (35). This comparison, listed in in Table 4 for each orifice, reveals how the difference between $\epsilon_{Reg}(f)$ and $\epsilon_{Irr}(f)$ may affect the total power extraction calculated. It can be seen that extraction efficiency $\tilde{\epsilon}_p$ is always slightly smaller than the corresponding value for ϵ_p. This minor difference can be due to two factors: (i) the minor difference between the values of $\epsilon_{Reg}(f)$ and $\epsilon_{Irr}(f)$ for each frequency as shown in Fig. 5, and (ii) the frequency range for $\epsilon_{Reg}(f)$ is only a truncated range for $\epsilon_{Irr}(f)$ due to the limitation of the facility used to perform tests using regular waves. It is important to highlight that $\epsilon_{Irr}(f)$ is not a true transfer function, as it is the spectral density of the measured signal. In this way, the frequency specific comparison of $\epsilon_{Reg}(f)$ and $\epsilon_{Irr}(f)$ carries uncertainty due to effects such as spectral leaking in $\epsilon_{Irr}(f)$ and the weak influence of wave amplitude on $\epsilon_{Reg}(f)$. We will argue in Discussion section that the truncation of the frequency range may have a more diminished impact on the total power extracted by the OWC, as the OWC may not be capable of extracting energy effectively from those frequencies outside the range used in the regular wave tests.

Since both R^2 and Skill values for $\epsilon_{Reg}(f)$ and $\epsilon_{Irr}(f)$ are all greater than 0.91 for all orifices and the difference between $\tilde{\epsilon}_p$ and ϵ_p is less than 10% for all orifices, we can conclude that for the range of frequencies tested in regular wave conditions, the hypothesis stated by Eq. (33) is confirmed by the data reported in Ulm et al.[18] for regular waves and the data present in this study for irregular waves.

It is concluded that that using the frequency-domain results from the regular wave tests can be used to estimate the performance of the OWC in irregular waves. Even though only one spectrum was examined here, the method should be applicable to other spectra as well with a similar degree of uncertainty.

Discussion

The proposed approximation method is based on the observation that the variation of the extraction efficiency found in regular wave conditions is not sensitive to variations in wave amplitude[18]. For practical application of this method, we need understand possible sources of uncertainty and how to use the proposed method to assist WEC developers to optimize their designs.

Sources of uncertainty

We will first assume that the duration of the irregular waves in the experimental is infinitely long, i.e., $T_d \to \infty$. According to Eq. (13), the total wave power extracted by an OWC can be calculated by

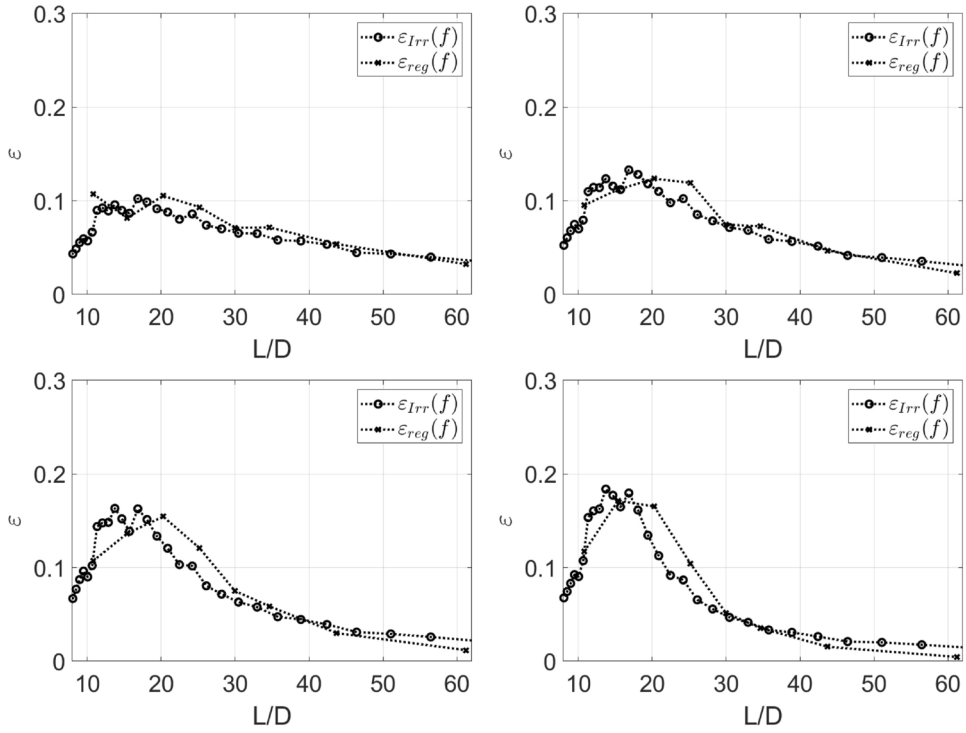


Fig. 5. Comparison of regular-wave extraction efficiency $\epsilon_{Reg}(f)$ found in Ulm et al.[18] and equivalent irregular-wave extraction efficiency $\epsilon_{Irr}(f)$ defined by Eq. (33). Results are presented relative to their variation with L/D for $\alpha = 0.5\%$ (Top Left), $\alpha = 0.7\%$ (Top Right), $\alpha = 1.0\%$ (Bottom Left), and $\alpha = 1.5\%$ (Bottom Right). L/D is the wave length L normalized by the size of the OWC chamber D.

Opening ratio (%) α	R^2	Skill
0.5	0.9715	0.9783
0.7	0.9556	0.9778
1.0	0.9117	0.9618
1.5	0.9255	0.9729

Table 3. Table of the R^2 between $\epsilon_{Reg}(f)$ reported in Ulm, et al.[18] and $\epsilon_{Irr}(f)$ calculated using Eq. (33).

Opening ratio (%) α	$\tilde{\epsilon}_p$	ϵ_p	$[\tilde{\epsilon}_p - \epsilon_p] / \epsilon_p$
0.5	0.0345	0.0383	-0.0992
0.7	0.0362	0.0389	-0.0694
1.0	0.0340	0.0345	-0.0145
1.5	0.0284	0.0285	-0.0035

Table 4. Comparison of the two methods to calculate the extraction efficiency: $\tilde{\epsilon}_p$ in frequency domain using results from regular wave tests and ϵ_p in time domain using irregular wave tests.

$$P_{OWC}^{tot} \equiv \int_{-\infty}^{\infty} \xi |p(t)|^{3/2} dt = \int_{0}^{\infty} P_{OWC}^{tot} \left(2|\hat{X}_{1/2}(f)|^2\right) df \tag{36}$$

Physically, the factor $2|\hat{X}_{1/2}(f)|^2$ determines how the wave power is extracted by each frequency component. We can rewrite the last term as a summation of two terms: the contribution within the frequency range $[f_L, f_H]$ and the contribution from frequency components outside this frequency range,

$$\int_{0}^{\infty} P_{OWC}^{tot} \left(2|\hat{X}_{1/2}(f)|^2\right) df = \int_{f_L}^{f_H} P_{OWC}^{tot} \left(2|\hat{X}_{1/2}(f)|^2\right) df + R \tag{37}$$

where the residual R is defined as

$$R = \int_0^{f_L} P_{OWC}^{tot}\left(2|\hat{X}_{1/2}(f)|^2\right) df + \int_{f_H}^{\infty} P_{OWC}^{tot}\left(2|\hat{X}_{1/2}(f)|^2\right) df > 0 \tag{38}$$

which is due to the truncation of the frequency range, and thus reduces with increasing the width of the frequency range $[f_L, f_H]$. For a well-designed OWC, the term R should be small as a well-designed OWC should be not efficient when the frequency is outside the frequency range of interest. It is remarked that direct calculation of R is not straight forward as the duration of irregular waves in a test is always finite. The nature of a finite test imposes limits on the range of frequencies tested, and thus require numerical implementations. In the case of the Welch periodogram method applied, the calculated spectrum suffers from windowing effects. In the following, we will try to confirm R/P_{OWC}^{tot} is reasonably small indirectly using our data.

The hypothesis stated by Eq. (33) allows us to make the following approximation within the frequency range $[f_L, f_H]$,

$$\int_{f_L}^{f_H} P_{OWC}^{tot}\left(2|\hat{X}_{1/2}(f)|^2\right) df = \int_{f_L}^{f_H} \epsilon_{Reg}(f)\left[D\rho g S_I(f) C_g(f)\right] df + \tilde{R}. \tag{39}$$

where the error $\tilde{R}$ is introduced by the difference between the values of $\epsilon_{Irr}(f)$ and $\epsilon_{Reg}(f)$ for any frequency in the range of $[f_L, f_H]$. The relative error in the last column of Table 4 suggests that $R + \tilde{R} > 0$. Theoretically, R is always positive. However, $\tilde{R}$ can be positive or negative. If the power extraction calculated using results from tests using regular waves underestimate the actual wave power extraction, i.e., $\tilde{R} > 0$, then both $|\tilde{R}|/P_{OWC}^{tot}$ and R/P_{OWC}^{tot} must be less than 10%. If the power extraction calculated using results from tests using regular waves overestimate the actual wave power extraction, i.e., $\tilde{R} < 0$, we can write $R = -\zeta\tilde{R}$ so that for the maximum ζ, we should have $(1-\zeta_{max})\tilde{R}/P_{OWC}^{tot} = 0.1$ as indicated by the results in Table 4, which means that Therefore, $\tilde{R}/P_{OWC}^{tot} = 0.1/(1-\zeta_{max}) < 0$. Since the difference between $\epsilon_{Irr}(f)$ and $\epsilon_{Reg}(f)$ is small as measured by R^2, which is always larger than 0.91, we may anticipate that $|\tilde{R}|/P_{OWC}^{tot} \sim 10\%$, which means that $\zeta_{max} \sim 2$ and $R/P_{OWC}^{tot} \sim 20\%$; however, in this case, the overestimation of the wave power extraction using results from tests based on regular waves can be partially compensated by the underestimation of the wave power extraction caused by the frequency truncation, as a result, the overall accuracy of the proposed method can be maintained at about 10%, which we believe is generic based on the following considerations: (i) the tests in regular wave and irregular waves conditions are independent, and (ii) the spectrum used in testing OWC in irregular wave conditions has two peaks, with one peak frequency being away from the peak frequency of $\epsilon_{Irr}(f)$ or $\epsilon_{Reg}(f)$, which potentially makes $\tilde{R}$ larger than that for a general spectrum with only one peak such as a JONSWAP spectrum. In the following discussion, we will assume the calculated power output will carry 10% uncertainty.

Sizing an OWC for given spectral waves using results obtained in regular wave conditions

For an OWC design, suppose we know $\epsilon_{Reg}(L/D)$ from either tests in regular waves conditions or frequency domain numerical simulations. A developer can use Eq. (34) to help determine the size of an OWC for a given design wave condition specified by a spectrum $S_I(f)$.

Note that in Eq. (34), the term $D\rho S_I(f)C_g(f)$ is the wave power per frequency available for the OWC to extract, which increases linearly with D, the size of the OWC. The shape of the extraction efficiency curve ϵ_{Reg} as a function of L/D is independent of the model size, but the curve of ϵ_{Reg} as a function of wave frequency f is dependent on the model size D. The extraction efficiency $\epsilon_{Reg}(L/D)$ can be expressed in terms of the wave frequency f, size of the OWC D as $\epsilon_{Reg}(L(f,h)/D)$ or $\epsilon_{Reg}(f,h,D)$, which means that for given frequency f and water depth h, the value of ϵ_{Reg} changes with D. Therefore, P_{OWC}^{tot} calculated using Eq. (34) is a function of D for a given OWC design and a specific design wave condition $S_I(f)$.

As an example, we consider ocean waves specified by a JONSWAP spectrum, which is expressed in terms of H_s and T_p as follows[49–51]:

$$S_I(f) = \beta_J \frac{H_s^2}{T_p^4 f^5} \exp\left[-1.25\left(T_p f\right)^{-4}\right]\gamma^{\delta}, \delta = \exp\left[-\frac{\left(T_p f - 1\right)^2}{2\sigma^2}\right] \tag{40}$$

where σ = 0.07 for $f < f_p$ and $\sigma = 0.09$ for $f \geq f_p$, and β_J is given by

$$\beta_J = \frac{0.0624(1.094 - 0.019\ln(\gamma))}{0.230 + 0.0336\gamma - 0.185(1.9+\gamma)^{-1}} \tag{41}$$

where γ is a peak enhancement factor in the range of 1 to 7. It has been found in the literature that the peak enhancement factor γ is affected by storm stage[52]: growing storms usually have a larger value of γ while decaying storms have of a smaller value of γ. Empirical relationships between the peak enhancement factor as a function of representative wave period and height have been proposed in the literature[53]. The following empirical relationship of the peak enhancement factor seems work reasonably well for all stages associated with storm waves based on available data[53],

$$\gamma = 8.54 H_s^{0.3} f_p^{0.7}. \tag{42}$$

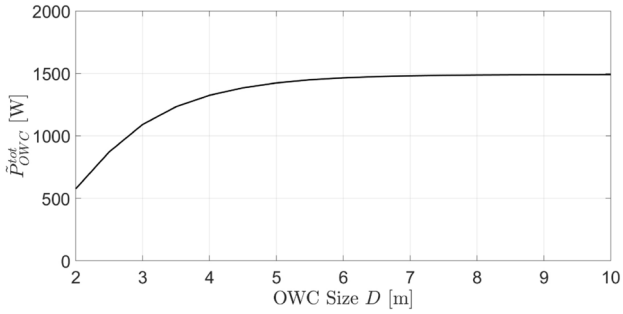


Fig. 6. Average power extracted from the spectral waves as OWC chamber diameter increases.

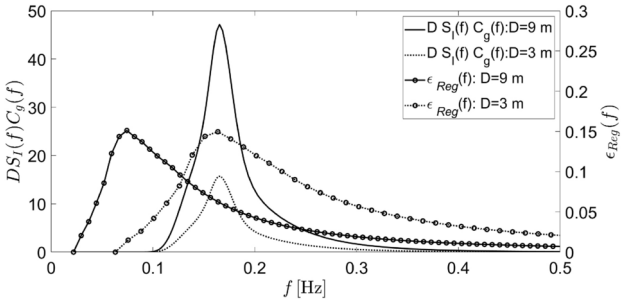


Fig. 7. Curves of $DS_I(f)C_g(f)$ and $\epsilon_{Reg}(f)$ for two values of *D*: 3 m and 9 m.

We assume that the WEC will be deployed at KNO in water of 20 m, and use the yearly averaged H_s = 1.0 m and T_p= 6.0 s as the design wave condition, which gives γ = 2.4 according to Eq. (42). We will used this value of γ for demonstration purpose. However, different empirical formulas for γ may give slightly different values. For example, DNV's design guideline[54] gives $\gamma = 1$ for the same wave condition. The total power extracted by the OWC studied here is shown in Fig. 6 as a function of the OWC size *D*, which is the diameter of the circular chamber. To produce the curve of $\epsilon_{Reg}(f)$ using that data for the opening ratio $\alpha = 1\%$, extrapolation was performed outside the frequency range tested based on the following requirements: $\epsilon_{Reg} = 0$ at $L/D = 0$ and 70. The extrapolation adopted here is supported by the results in previous studies of circular OWCs[17].

Note that there is a plateau between D = 5 m and D = 10 m, which means that the amount of pneumatic power extracted varies little when D varies between 5m and 10m. However, the cost for a 10m OWC is much more higher than that for a 5m OWC. This poses a question about criteria we should use to optimize the size of an OWC: power output is one criterion, the cost should be another criterion to consider. One metric to measure the competitiveness of a WEC design is the concept of levelized cost of energy[5], wwhich may be affected by many factors such as costs for material, labor, transportation as well as the geotechnical features of the seabed where a WEC is to be installed. We use the pneumatic power output at D =9m as a reference, which is about 1500W, a sacrifice of the power output by 25% can reduce the OWC size from 9 m to 3 m. Since the wave loading and the amount of materials needed to construct the OWC is scaled by λ^3 with λ being the geometric scale factor, the weight or loading for the OWC of size D =3 m is just about 2% of that for the OWC of size D =9 m. The significant reduction in material and wave loading will come with a significant reduction in costs associated with manufacturing, transportation, labor and installation. If we assume that the average power requirement for this application is about 1.5 kW, the best size for the design wave condition might be D =3m, which means we should deploy two 3m WECs, installed of one 9m WEC to meet the power need.

The reason the curve $\tilde{P}^{tot}_{OWC}(D)$ becomes relative flat when D >5m can be understood by examining the curves of $DS_I(f)C_g(f)$ and $\epsilon_{Reg}(f, h, D)$ as functions of *f* for different values of *D*. Note that the curve of $D\rho g S_I(f)C_g(f)$, which represents the wave power available for extraction by the OWC of size *D* per frequency, can be represented by that of $DS_I(f)C_g(f)$ since both ρ and *g* are constant. Fig. 7 shows two curves of $\epsilon_{Reg}(f)$ and two curves of $DS_I(f)C_g(f)$ for opening ratio $\alpha = 1\%$, with the two representative values of *D*:3m and 9m. The peak of $\epsilon_{Reg}(f)$ represents a natural frequency of the OWC system, thus it decreases with increasing the size of the OWC structure. On the other hand, increasing *D* only linearly increases the amount of wave power available for OWC to extract, and thus will not change the peak location of $D\rho S_I(f)C_g(f)$. It can be seen that when the size of the OWC makes the peak of $\epsilon_{Reg}(f, h, D)$ close to the peak of $DS_I(f)C_g(f)$, which occurs at D_{opt} ~3m, the OWC does not necessarily perform better because the amount of wave power that is available for the OWC to extract is small because of the small size of the OWC. The reason why the curve $\tilde{P}^{tot}_{OWC}$ has a plateau is because increasing *D* causes the following two completing effects as shown in Fig. 7: (i) moves the peak of $\epsilon_{Reg}(f, h, D)$ towards the low frequency side, resulting in a reduce efficiency of the OWC at the peak

frequency of the wave spectrum; (ii) increases the total wave power available for the OWC to extract at the peak of the wave spectrum. As a result, a plateau occurs.

Estimating seasonal variability of an OWC using Results Obtained in Regular Wave Conditions

After the size of an OWC is selected, a WEC developer can use Eq. (34) to estimate the seasonal variability of the OWC performance by using a different $S_I(f)$ for each season because $\epsilon_{Reg}(L/D)$ is largely a property of the OWC, independent of the wave conditions. In this case, a developer could fix $\epsilon_{Reg}(L/D)$ and D, but vary T_p and H_s according to wave data for the project site.

Applicability of the Method for Floating OWCs

The primary focus of this study is to evaluate the methods used to assess power performance for a fixed OWC. It is worth noting that the presented results were a part of multifaceted experiments, where a floating variation of the model was tested concurrently. For floating OWCs, the motion response can also influence power production. The applicability of the method presented in this study for the floating OWC will be evaluated, and the results will be presented in a future publication.

Scale effects

The Reynolds similarity and modeling laws related to air compressibility were not considered in the experiment, which may introduce some scale effects. For small scale models with an orifice as an PTO, the influence of the compressibility of the air in the OWC chamber can be ignored[17]. For large models, air compressibility may affect the extraction efficiency as much as 10%[12,55]. This uncertainty may slightly change the rate of plateau of an efficiency curve but would not change the conclusion.

Conclusion

This study experimentally examined the power performance of an OWC geometry with a submerged heave plate and V-shaped channels in irregular wave conditions. The experiment was conducted in a large-scale wave basin. Influence of characteristics of PTO on power extraction was examined by using sharp-edged orifices of different opening ratios. Four opening ratios ranging from 0.5% to 1.5% were examined in the experiment. The results confirmed that (i) the orifice characteristics obtained from tests in regular waves are in good agreement with those obtained in irregular waves, and (ii) the power extraction can be accurately calculate using the pressure measured in the OWC chamber. A new method of estimating total power extraction of an OWC in irregular wave conditions was proposed, which relies on the results obtained from tests of the same OWC in regular waves. The method was verified by a comparison of the results from the tests of the same OWC model in regular and irregular waves. A discussion of the uncertainty associated with the proposed method revealed a about 10% uncertainty in the power output estimated by the proposed method. An example was also discussed about how to use the proposed method to determine the optimal size of an OWC for a given wave condition specified by a JONSWAP spectrum, an the discussion suggested that the optimal size of an OWC needs to be determined based on the total power output as well as structure size, the wave loading and cost. Matching the peak of the efficiency curve of an OWC with the peak of the spectrum may not produce an optimal OWC. There is a need to further verify the proposed method using data collected for different types of OWCs to prove the method's robustness.

Data availability

The datasets used and/or analysed during the current study are available from the corresponding author on reasonable request.

Received: 14 October 2024; Accepted: 13 February 2025
Published online: 19 March 2025

References

1. LiVecchi, A. et al. *Powering the Blue Economy; Exploring Opportunities for Marine Renewable Energy in Maritime Markets* (U.S., Department of Energy, Office of Energy Efficiency and Renewable Energy, 2019).
2. Falnes, J. A review of wave-energy extraction. *Mar. Struct.* **20**, 185–201. https://doi.org/10.1016/j.marstruc.2007.09.001 (2007).
3. Falcão, A. F. D. O. Wave energy utilization: A review of the technologies. *Renew. Sustain. Energy Rev.* **14**, 899–918. https://doi.org/10.1016/j.rser.2009.11.003 (2010).
4. Xu, C. & Huang, Z. A dual-functional wave-power plant for wave-energy extraction and shore protection: A wave-flume study. *Appl. Energy* **229**, 963–976 (2018).
5. Calheiros-Cabral, T. et al. Evaluation of the annual electricity production of a hybrid breakwater-integrated wave energy converter. *Energy* **213**, 118845. https://doi.org/10.1016/j.energy.2020.118845 (2020).
6. Evans, D. & Porter, R. Efficient calculation of hydrodynamic properties of owc-type devices. *J. Offshore Mech. Arct. Eng.* **119**, 210–218. https://doi.org/10.1115/1.2829098 (1997).
7. Falcão, A. F. O. & Henriques, J. C. C. Oscillating-water-column wave energy converters and air turbines: A review. *Renew. Energy* **85**, 1391–1424. https://doi.org/10.1016/j.renene.2015.07.086 (2016).
8. He, F. & Huang, Z. Hydrodynamic performance of pile-supported owc-type structures as breakwaters: An experimental study. *Ocean Eng.* **88**, 618–626. https://doi.org/10.1016/j.oceaneng.2014.04.023 (2014).
9. *Islay Limpet Wave Power Plant* (1998).
10. Henriques, J. C. C. et al. Design of oscillating-water-column wave energy converters with an application to self-powered sensor buoys. *Energy* **112**, 852–867. https://doi.org/10.1016/j.energy.2016.06.054 (2016).
11. Viviano, A., Musumeci, R. E., Vicinanza, D. & Foti, E. Pressures induced by regular waves on a large scale owc. *Coast. Eng.* **152**, 103528. https://doi.org/10.1016/j.coastaleng.2019.103528 (2019).

12. Weber, J. Representation of non-linear aero-thermodynamic effects during small scale physical modelling of oscillating water column wave energy converters. In *Seventh European Wave and Tidal Energy Conference* (2007).
13. IEA-OES. Annual report: An overview of ocean energy activities in 2023. Tech. Rep., (International Energy Agency, 2024).
14. Xu, C. & Huang, Z. Three-dimensional CFD simulation of a circular owc with a nonlinear power-takeoff: Model validation and a discussion on resonant sloshing inside the pneumatic chamber. *Ocean Eng.* **176**, 184–198. https://doi.org/10.1016/j.oceaneng.2019.02.010 (2019).
15. Huang, Z. & Huang, S. Two-phase flow simulations of fixed 3D oscillating water columns using openfoam: A comparison of two methods for modeling quadratic power takeoff. *Ocean Eng.* **232**, 108600. https://doi.org/10.1016/j.oceaneng.2021.108600 (2021).
16. Zhao, M. & Ning, D. A review of numerical methods for studying hydrodynamic performance of oscillating water column (owc) devices. *Renew. Energy* **233**, 121177. https://doi.org/10.1016/j.renene.2024.121177 (2024).
17. Xu, C., Huang, Z. & Deng, Z. Experimental and theoretical study of a cylindrical oscillating water column device with a quadratic power take-off model. *Appl. Ocean Res.* **57**, 19–29. https://doi.org/10.1016/j.apor.2016.02.003 (2016).
18. Ulm, N., Huang, Z. & Cross, P. Experimental study of a fixed owc-type wave energy converter with a heave plate and v-shaped channels for intermediate-water-depth applications. *Energies* **16**, 5988. https://doi.org/10.3390/en16165988 (2023).
19. He, F., Li, M. & Huang, Z. An experimental study of pile-supported owc-type breakwaters: Energy extraction and vortex-induced energy loss. *Energies* **9**, 540. https://doi.org/10.3390/en9070540 (2016).
20. Falcão, A. F. O., Henriques, J. C. C. & Candido, J. J. Dynamics and optimization of the owc spar buoy wave energy converter. *Renew. Energy* **48**, 369–381. https://doi.org/10.1016/j.renene.2012.05.009 (2012).
21. Borriello, A. et al.*The EU blue economy report 2024* (Publications Office of the European Union, European Commission and Directorate-General for Maritime Affairs and Fisheries and Joint Research Centre, 2024).
22. He, F. & Huang, Z. Characteristics of orifices for modeling non-linear power takeoff in wave flume tests of oscillating water column devices. *Zhejiang Univ. Sci. A Appl. Phys. Eng.* **18**, 329–345. https://doi.org/10.1631/jzus.A1600769 (2017).
23. Tseng, R.-S., Wu, R.-H. & Huang, C.-C. Model study of a shoreline wave-power system. *Ocean Eng.* **27**, 801–821. https://doi.org/10.1016/S0029-8018(99)00028-1 (2000).
24. Gouaud, F., Rey, V., Piazzola, J. & Hooff, R. Experimental study of the hydrodynamic performance of an onshore wave power device in the presence of an underwater mound. *Coast. Eng.* **57**, 996–1005. https://doi.org/10.1016/j.coastaleng.2010.06.003 (2010).
25. Deng, Z., Ou, Z., Ren, X., Zhang, D. & Si, Y. Theoretical analysis of an asymmetric offshore-stationary oscillating water column device with bottom plate. *J. Water. Port Coast. Ocean Eng.* **146**, 574. https://doi.org/10.1061/(ASCE)WW.1943-5460.0000574 (2020).
26. Fleming, A. N. & Macfarlane, G. J. Experimental flow field comparison for a series of scale model oscillating water column wave energy converters. *Mar. Struct.* **52**, 108–125. https://doi.org/10.1016/j.marstruc.2016.12.005 (2017).
27. Elhanafi, A., Macfarlane, G., Fleming, A. & Leong, Z. Experimental and numerical investigations on the hydrodynamic performance of a floating-moored oscillating water column wave energy converter. *Appl. Energy* **205**, 369–390. https://doi.org/10.1016/j.apenergy.2017.07.138 (2017).
28. Wang, C. & Zhang, Y. Numerical investigation on the wave power extraction for a 3d dual-chamber oscillating water column system composed of two closely connected circular sub-units. *Appl. Energy* **295**, 117009. https://doi.org/10.1016/j.apenergy.2021.117009 (2021).
29. Oikonomou, C. L., Gomes, R. P. & Gato, L. M. Unveiling the potential of using a spar-buoy oscillating-water-column wave energy converter for low-power stand-alone applications. *Appl. Energy* **292**, 116835. https://doi.org/10.1016/j.apenergy.2021.116835 (2021).
30. Falcão, A. F. D. O. & Rodrigues, R. J. A. Stochastic modelling of owc wave power plant performance. *Appl. Ocean Res.* **24**, 59–71. https://doi.org/10.1016/S0141-1187(02)00022-6 (2002).
31. Ahn, S. Modeling mean relation between peak period and energy period of ocean surface wave systems. *Ocean Eng.* **228**, 108937. https://doi.org/10.1016/j.oceaneng.2021.108937 (2021).
32. Liu, Z., Xu, C., Shi, H. & Qu, N. Wave-flume tests of a model-scaled owc chamber-turbine system under irregular wave conditions. *Appl. Ocean Res.* **99**, 102141. https://doi.org/10.1016/j.apor.2020.102141 (2020).
33. Davidson, J., Henriques, J. C. C., Gomes, R. P. F. & Galeazzi, R. Opening the air-chamber of an oscillating water column spar buoy wave energy converter to avoid parametric resonance. *IET Renew. Power Gener.* **15**, 3109–3125. https://doi.org/10.1049/rpg2.12204 (2021).
34. Babarit, A. A database of capture width ratio of wave energy converters. *Renew. Energy* **80**, 610–628. https://doi.org/10.1016/j.renene.2015.02.049 (2015).
35. Viviano, A., Naty, S. & Foti, E. Scale effects in physical modelling of a generalized owc. *Ocean Eng.* **162**, 248–258. https://doi.org/10.1016/j.oceaneng.2018.05.019 (2018).
36. Falcão, A. F. O. & Henriques, J. C. C. Model-prototype similarity of oscillating-water-column wave energy converters. *Int. J. Mar. Energy* **6**, 18–34. https://doi.org/10.1016/j.ijome.2014.05.002 (2014).
37. ISO-5167-2:2022. Measurement of fluid flow by means of pressure differential devices inserted in circular cross-section conduits running full-part 2: Orifice plates. Standard, (International Organization for Standardization, 2022).
38. Hughes, S. A. *Physical Models and Laboratory Techniques in Coastal Engineering* (World Scientific, 1993).
39. Hebert, A. B., Sansone, F. J. & Pawlak, G. R. Tracer dispersal in sandy sediment porewater under enhanced physical forcing. *Cont. Shelf Res.* **27**, 2278–2287. https://doi.org/10.1016/j.csr.2007.05.016 (2007).
40. Johansen, F. C. Flow through pipe orifices at low reynolds numbers. *Proc. R. Soc. A* **126**, 231–245. https://doi.org/10.1098/rspa.1930.0004 (1930).
41. Mei, C., Stiassnie, M. & Yue, D. *Theory and Applications of Ocean Surface Waves* (World Scientific, 2005).
42. Willmott, C. J. On the validation of models. *Phys. Geogr.* **1**, 184–194 (1981).
43. Guillou, N. Estimating wave energy flux from significant wave height and peak period. *Renew. Energy* **155**, 1383–1393 (2020).
44. Welch, P. The use of fast Fourier transform for the estimation of power spectra: A method based on time averaging over short, modified periodograms. *IEEE Trans. Audio Electroacoust.* **15**, 70–73 (1967).
45. Bartlett, M. S. Smoothing periodograms from time-series with continuous spectra. *Nature* **161**, 686–687 (1948).
46. Hayes, M. H. *Statistical Digital Signal Processing and Modeling* (Wiley, 1996).
47. Ifeachor, E. C. & Jervis, B. W. *Digital Signal Processing: A Practical Approach* (Pearson Education, 2002).
48. Massel, S. R. *Ocean Surface Waves: Their Physics and Prediction* (World Scientific, 1996).
49. Goda, Y. *Random Seas and Design of Maritime Structures* (World scientific, 2010).
50. Mazzaretto, O. M., Menéndez, M. & Lobeto, H. A global evaluation of the jonswap spectra suitability on coastal areas. *Ocean Eng.* **266**, 112756 (2022).
51. Hwang, S., Lim, C. & Lee, J. L. Extraction of nearshore spectrum by energy-conserved zero-up crossing method and comparison with the tma spectrum. *Ocean Eng.* **241**, 109962 (2021).
52. Ewans, K. & McConochie, J. Optimal methods for estimating the jonswap spectrum peak enhancement factor from measured and hindcast wave data. In *International Conference on Offshore Mechanics and Arctic Engineering*, vol. 58783, V003T02A046 (American Society of Mechanical Engineers, 2019).
53. Mazaheri, S. & Imani, H. Evaluation and modification of jonswap spectral parameters in the persian gulf considering offshore wave characteristics under storm conditions. *Ocean Dyn.* **69**, 615–639 (2019).
54. Veritas, D. N. *Recommended Practice: Environmental Conditions and Environmental Loads* (DNV-GL, 2010).

55. López, I., Carballo, R., Taveira-Pinto, F. & Iglesias, G. Sensitivity of owc performance to air compressibility. *Renew. Energy* **145**, 1334–1347. https://doi.org/10.1016/j.renene.2019.06.076 (2020).

Acknowledgements
This material is based upon work partially supported by the NAVAL SEA SYSTEMS COMMAND (NAVSEA) under Contract No. N00024-19-D-6400, Task Order No. 20F8819-WETS 5. Funding for facility time was through the U.S. Testing Expertise and Access for Marine Energy Research Program (TEAMER). This material is based upon work partially supported by the U.S. Department of Energy's Office of Energy Efficiency and Renewable Energy (EERE) under the Water Power Technologies Office Award Number DE-EE0008895. Special thanks to the students and staff at Oregon State University: Pedro Lomonaco, Bret Bosma, Tim Maddux, Jonah Gadasi, Shangyan Zou, and Courtney Beringer for assistance in facilitating testing. We thank Duncan Lajousky and Reza Ghorbani from the University of Hawaii for their contributions to the development and testing of the OWC model. We thank Geno Pawlak at the University of California San Diego for providing us with wave data from the Kilo Nalu Observatory. This is SOEST contribution no. 11905.

Author contributions
Conceptualization, N.U., Z.H. and P.C.; methodology, N.U. and Z.H.; software, N.U.; validation, N.U.; formal analysis, N.U.; investigation, N.U. and Z.H.; resources, P.C.; data curation, N.U.; writing-original draft preparation, N.U. and Z.H.; visualization, N.U.; supervision, Z.H.; project administration, P.C.; funding acquisition, P.C. All authors have read and agreed to the published version of the manuscript.

Declarations

Competing interests
The authors declare no competing interests. The funders had no role in the design of the study; in the collection, analyses, or interpretation of data; in the writing of the manuscript; or in the decision to publish the results. This manuscript was prepared as an account of work sponsored by an agency of the United States Government. Neither the United States Government nor any agency thereof, nor any of their employees, makes any warranty, express or implied, or assumes any legal liability or responsibility for the accuracy, completeness, or usefulness of any information, apparatus, TEAMER Program Special Terms and Conditions Page 7 of 19 4814-2710-6234.4 product, or process disclosed, or represents that its use would not infringe privately owned rights. Reference herein to any specific commercial product, process, or service by trade name, trademark, manufacturer, or otherwise does not necessarily constitute or imply its endorsement, recommendation, or favoring by the United States Government or any agency thereof. The views and opinions of authors expressed herein do not necessarily state or reflect those of the United States Government or any agency thereof.

Additional information
Correspondence and requests for materials should be addressed to Z.H.

Reprints and permissions information is available at www.nature.com/reprints.

Publisher's note Springer Nature remains neutral with regard to jurisdictional claims in published maps and institutional affiliations.

Open Access This article is licensed under a Creative Commons Attribution-NonCommercial-NoDerivatives 4.0 International License, which permits any non-commercial use, sharing, distribution and reproduction in any medium or format, as long as you give appropriate credit to the original author(s) and the source, provide a link to the Creative Commons licence, and indicate if you modified the licensed material. You do not have permission under this licence to share adapted material derived from this article or parts of it. The images or other third party material in this article are included in the article's Creative Commons licence, unless indicated otherwise in a credit line to the material. If material is not included in the article's Creative Commons licence and your intended use is not permitted by statutory regulation or exceeds the permitted use, you will need to obtain permission directly from the copyright holder. To view a copy of this licence, visit http://creativecommons.org/licenses/by-nc-nd/4.0/.

© The Author(s) 2025